Middle-East Journal of Scientific Research 25 (7): 1438-1445, 2017
ISSN 1990-9233

DOI: 10.5829/idosi.mejsr.2017.1438.1445

Investigation of Resting-state Hemispheric Asymmetry in the Default Mode Network

Hongxia Li

School of Economics and Management, Tsinghua University, Beijing 100875, China

Abstract: Previous studies have demonstrated left and right asymmetry patterns in the human brain. A recent study showed that hemispheric asymmetries of the left and right brain are commonly observed in multiple functional magnetic resonance imaging (fMRI) studies. However, the differences between the left and right brain resting-state activity levels with respect to the directions and strengths of causal interactions among the nodes in the default mode network (DMN) remain unknown. In this study, we sought to build on the findings of previous studies by detecting the differences in the directions and strength of causal interactions between the left and right hemispheres in the DMN. Twenty-four healthy right-handed volunteers were recruited for this study. The DMN was extracted using ICA and seven cortical regions were identified. We investigated the causal interactions within the seven nodes in the DMN by applying the mGCA. A causal connectivity network graph was depicted using the arrow-headed lines of varying thickness to illustrate the directions and strengths of the causal influences. The activity levels measured by the In-Out degree with path weight varied across the regions, which were sorted according to their In-Out degrees of effective connectivity with path weight in descending order: vMPFC > dMPFC > PCC > lANG > rANG > rIPL > lIPL. These results highlight the presence of clear asymmetries between the left and right brain in the DMN using mGCA. These findings have significant implications for understanding of the functional and structural hemispheric asymmetries in the human brain.

Key words: Hemispheric asymmetry · Resting-state fMRI · Default mode networks · Independent component analysis · Multivariate Granger causality analysis

INTRODUCTION

Hemispheric asymmetries have been discovered via brain anatomical, functional and behavior studies [1]. It is of great significance that differences in the left and right hemispheres can reveal the mechanisms of cognitive language, visual perception and sensory function processing in the brain [2, 3]. Previous studies have shown that significant differences in the left and right hemispheres can be detected in some brain cortices [3, 4]. For example, a left-greater-than-right asymmetry pattern along the cingulum bundles was revealed [5].

Hemispheric asymmetries between the left and right brain were observed in multiple functional magnetic resonance imaging (fMRI) studies [6], including in a resting-state fMRI study [7]. Resting-state networks in the human brain, such as the default mode network (DMN), have been extensively reported. Fluctuations in the blood oxygenation level-dependent (BOLD) signal during the resting state reflect the neuronal baseline activity of the brain, indicating the state of the human brain in the absence of goal-directed neuronal action and external input. Furthermore, these slow fluctuations correspond to functionally relevant resting-state networks [8].

Functional imaging studies have revealed coactivation in a distributed network of cortical regions that characterizes the resting state, or default mode, of the human brain. The DMN is comprised of a set of cortical and subcortical regions, including the posterior cingulate/precuneus cortices (PCC/PrCC), medial prefrontal cortex (MPFC), orbital frontal gyrus, anterior cingulate gyrus, inferotemporal cortex and lateral parietal cortex [9,10]. It is highly heterogeneous in that the active levels of the DMN in different areas are characterized by the magnitude of the low frequency (0.01–0.08 Hz) of BOLD signal fluctuations [11]. The DMN may ultimately be used as a biomarker for certain pathological changes in the human brain [10]. In a resting-state fMRI study [12], the authors demonstrated that the connectivity strength

Corresponding Author: Hongxia Li, Room # 413, Weilun Building, School of Economics and Management, Tsinghua University, Beijing 100084, China.

within the anterior cingulate cortex is significantly greater in the right hemisphere than in the left. However, the differences in the directions and strengths of the causal interactions among the nodes in the DMN between the resting-state activity levels of the left and right brain remain unknown.

In this study, we combined independent component analysis (ICA) and multivariate Granger causality analysis (mGCA) to explore the causal interactions between the nodes in the DMN. The mGCA was applied to evaluate the effective connectivity and strengths between the brain regions, as this type of analysis can detect direct causal interactions within the networks by calculating the directed transfer function (DTF) from a multivariate autoregressive (MVAR) model [13]. In particular, we sought to extend the previous studies by exploring whether there are differences in the directions and strengths of causal interactions between the left and right hemispheres in the DMN. We expected to provide additional evidence in support of hemispheric asymmetries in the human brain and offer a new approach for detecting brain damage in a clinical setting.

MATERIALS AND METHODS

Subjects: Twenty-four healthy Chinese right-handed volunteers (9 males, mean age: 24.1 ± 0.9 years; 15 females, mean age: 23.9± 0.8), with no history of neurological or psychiatric disorders, were recruited for this study. None of the subjects had taken prescription medications within the last month of the study, nor did they have any contraindications for exposure to a high magnetic field. All subjects were right handed and provided written informed consent to participate in this study, as approved by the local Ethics Committee. All experiments were in accord with the Declaration of Helsinki.

Data Acquisition and Analysis: All subjects underwent a 6-min scan in the resting state. During the experiment, subjects were instructed to keep their eyes closed and remain relaxed without engaging in any mental tasks. All fMRI data were acquired on a 1.5-Tesla ACS-NT 15 Philips scanner (Best, Netherlands) equipped with a standard head coil. A custom-built holder prevented head movements during the scans. Whole-brain images were acquired parallel to the anterior commissure-posterior commissure line. Thirty axial slices were obtained using a T2*-weighted single-shot and gradient-recalled echo planar imaging sequence (field of view [FOV] = 230 × 230mm^2, matrix = 64 × 64, thickness = 5 mm [0 mm gap], repetition time [TR] =2000 ms, echo time [TE] = 50 ms, flip angle = 90). After the functional images were acquired, high-resolution structural scans were performed on each subject for anatomical localization using three-dimensional MRI sequences with a voxel size of 1 mm^3 (TR = 2510 ms, TE = 15 ms, matrix = 384 × 512, FOV = 230 × 230 mm^2, flip angle = 30°, thickness = 5 mm).

To eliminate the nonequilibrium effects of magnetization, the first five volumes were discarded [14]. Next, all of the images were preprocessed using statistical parametric mapping (SPM5, http://www.fil.ion.icl.ac.uk/spm/). First, the images were realigned for head motion using least-squares minimization. None of subjects had head movements exceeding 1 mm in any direction or head rotation greater than 1°. A mean image created from the realigned volumes was coregistered with the subject's individual structural T1-weighted volume image. The standard Montreal Neurological Institute (MNI) template provided by SPM5 was used in spatial normalization with resampling at 2 × 2 × 2 mm. A bandpass filter (0.01–0.08 Hz) was applied to reduce the effect of low-frequency drift and high-frequency noise [11]. Finally, to spatially smooth the functional images, an isotropic Gaussian kernel (full-width at half-maximum = 6 mm) was applied.

ICA: We performed a group spatial ICA operation on the smoothed data from all subjects during the 6-min resting state scan using the fMRI Toolbox (GIFT, http://icatb.sourceforge.net/). Principal component analysis was used to reduce the images to 40 dimensions and the number of independent components (ICs) was estimated to be 25 using the minimum description length criteria [15]. To indicate the voxel that contributed most strongly to a particular IC, the intensity values in each spatial map were converted to *Z* values. The ICs corresponding to the DMN were extracted based on templates described previously [16]. Once the ICA separation was complete, the DMN templates were used to select the low-frequency components in each subject using a best-fit procedure [10]. Briefly, a template-matching procedure was used by taking the average *Z* value of voxels falling within the template minus the average *Z* values of voxels outside the template and selecting the component in which this difference (the goodness-of-fit) was the greatest. The *Z* values used here reflect the degree to which a given voxel's time series correlates with the time series corresponding to a specific ICA component, scaled by the standard deviation of the error term. The ICs corresponding to the DMN were

extracted from all subjects. Then, *Z*-maps of the DMN were generated for a random effects analysis using a one-sample *t*-test ($P < .05$).

ROI Definition: In the current study, the regions of interest (ROIs) for the key DMN nodes were determined using the Marsbar software package (http://marsbar.sourceforge.net). ROIs were defined as the set of voxels included in the 8-mm spheres centered on the local maximum activation clusters extracted from the ICA. The averaged resting BOLD signal over the voxels in each ROI along the 90 TRs was considered the time course of the ROI. The time series were averaged across the voxels within each ROI, for each subject, to form a single vector per ROI. In this manner, we obtained a total of 24 × 7 ROI time series for further analysis.

mGCA: Previous neuro-imaging studies suggest that mGCA is an effective way to investigate the causal networks [17]. Here, we only considered the effective connectivity patterns of the resting state. Let $\mathbf{X}(t) = (x_1(t), x_2(t), ..., x_N(t))^T$ be a matrix representing data from the summary time series of the ROIs. Here, $x_i(t)$ $(i = 1, ..., N)$ is a time series corresponding to the *i*th ROI and *T* denotes matrix transposition. Bold letters represent time domain matrices and capital letters in normal font denote their frequency domain counterparts. The MVAR model of the order *p* is given by

$$\mathbf{X}(t) - \sum_{n=1}^{p} \mathbf{A}(n)\mathbf{X}(t-n) = \mathbf{E}(t) \tag{1}$$

Where A(*n*) is the matrix of model parameters consisting of elements $a_{ij}(n)$ and E(*t*) is the vector corresponding to the residual error. The Schwarz criterion was used to set the order of the autoregressive model to 1 [17]. Then, equation [1] was transformed to the frequency domain as follows:

$$X(f) = A^{-1}(f)E(f) = H(f)E(f) \tag{2}$$

$$H(f) = A^{-1}(f) \tag{3}$$

where $a_{ij}(f) = \delta_{ij} - \sum_{n=1}^{p} a_{ij}(n)e^{-i2\pi fn}$ and the element a_{ij} correspond to matrix *A*.

Here, δ_{ij} is the delta function, expressed as $\delta_{ij} = \begin{cases} 1, & i = j, \\ 0, & i \neq j. \end{cases}$. Additionally, $i = 1...N, j = 1...N$. $H(f)$ is the frequency domain transfer matrix and $h_{ij}(f)$ represents its element in the *i*th row and *j*th column. $h_{ij}(f)$ is defined as the non-normalized DTF corresponding to the influences of ROI *j* to ROI *i* [18]. The direct DTF (dDTF) is obtained by multiplying $h_{ij}(f)$ with the partial coherence between ROIs *i* and *j*. This operation emphasizes the direct causality rather than the mediated influences.

To calculate the partial coherence, the cross-spectra are computed as

$$S(f) = H(f)VH^H(f) \tag{4}$$

Here, *V* is variance of the matrix $E(f)$ and *H* in the upper right corner denote conjugate transpose. Next, we obtained the partial coherence between ROIs *i* and *j* using

$$\theta_{ij}(f) = \frac{M_{ij}^2(f)}{M_{ii}(f)M_{jj}(f)} \tag{5}$$

where $M_{ij}(f)$ is the cofactor of matrix S. The partial coherence is confined to the range of [0, 1]. If the value is zero, this indicates that there is no statistically significant direct relation between a pair of ROIs; however, if the value is one, this indicates a complete direct association. The dDTF is defined as the sum of the frequency components of the product of the non-normalized DTF and partial coherence, as given in the equation below:

$$dDTF_{ij} = \sum_{f} h_{ij}(f)\theta_{ij}(f) \tag{6}$$

Eventually, the dDTF value was obtained, which reflects the magnitude of the causal influences between ROIs.

To assess the significance of path weights, a null distribution was obtained by generating 2500 sets of surrogate data and the dDTF was calculated from these data sets [19]. The dDTF value was compared with the null distribution using a one-tailed test of significance with a *P* value of.05. The effective connectivity network of the 12 ROIs was constructed by scaling the significant dDTF values.

To compare the relative information flow in the three mGCA networks, the measure of In-Out degree was applied. The In-degree of a node in a causal connectivity network is defined as the number of causal in-flow connections to the node from any of the other nodes in the network. The Out-degree of a node refers to the number of causal out-flow connections from the node to any of the other nodes in the network. In the present study, the In-Out degree of a node was a novelty and was

defined as the difference between the numbers of causal in-flows and out-flows with path weight [11].

Statistical Analyses: The distributions of mGCA are not established because they may have a highly nonlinear relationship with the time series data [20]. Therefore, to assess the significance of the Granger causality reflected by the dDTF, we employed surrogate data [18,19,20] to obtain an empirical null distribution. The original time series was transformed into the frequency domain and their phase was uniformly distributed over $(-\pi,\pi)$ [18]. Then, to generate the surrogate data, the signal was transformed back to the time domain. This procedure ensured that the surrogate data maintained the same spectrum as the original data, but with the causal phase relations destroyed. The dDTF was calculated between the surrogate data time series representing each ROI. By repeating the above procedure 2500 times, null distributions were derived for all possible connections between the ROIs for each subject. For each connection, the actual dDTF was compared with its corresponding null distribution to derive a *P* value. To establish group significance inferences, the *P* values from individual subjects were combined using Fisher's method [20] to obtain a single *P* value.

RESULTS

In this work, the DMN was extracted using ICA and seven cortical regions were identified for further analysis including the PCC/PrCC, dorsal MPFC (dMPFC), ventral MPFC (vMPFC), left angular gyrus (lANG), right angular gyrus (rANG), left inferior parietal lobule (lIPL) and right inferior parietal lobule (rIPL). The spatial independent component in the DMN of the group results is represented with slices (Fig. 1). All images are *Z* statistics (Table 1) overlaid on the average high-resolution scan transformed into standard (MNI152) space. Red to yellow in the bar represents the *Z* values, ranging from 1.5 to 9.0 (Fig. 1).

We investigated the causal interactions within the seven nodes in the DMN by applying the mGCA. The effective connectivity patterns of brain networks were described as "directed graphs." The thickness of the connecting lines and the directions of the arrows (Fig. 2) indicated the directions and strengths of the causal influences, respectively. Significant effective connectivity was divided into four levels (25%, 50%, 75% and 100%) relative to the maximum significant dDTF value, which are presented in the graph. These connections demonstrated significant Granger causal connectivity at the group level (Fisher's method, $P < .05$) (all significant black line in Fig. 2).

The directions and strengths of the causal influences coming into, or going from, each node were different within the network. In particular, several distinct inconsistent connections in the left and the right hemispheres were found. A direct connection emerges from the rANG to the PCC at the weak strength of 25% significant effective connectivity, but no direct connections exist between the lANG and PCC. A direct connection emerges from the lANG to the rANG at the weak strength of 25%, while a connection from the rANG to the lANG exists at the strength of 50%. A direct connection emerges from the lANG to the vMPFC at the strength of 50%, while the connection from the rANG to the vMPFC emerges at the weak strength of 25%. There was a direct connection from the lIPL to the dMPFC at the strength of 25%, while no direct connections between the rIPL and dMPFC were observed. A direct connection emerges from the lIPL to the lANG at the strong strength of 100%, while the connection from the rIPL to the rANG had a strength of 75%. A direct connection emerges from the lIPL to the rANG at the strength of 75%,

Table 1: Coordinates and Z values of the peak voxel within group ROIs during the resting state ($P < .05$, false discovery rate corrected).

	Talairach				Z	V
Regions	x	y	z	BA	Value	Voxels
dMPFC	-2	56	-7	10	2.81	133
vMPFC	-2	48	-20	10	3.70	127
PCC	0	-53	21	23	4.37	977
lANG	-46	-72	30	39	2.29	60
rANG	48	-72	30	39	2.73	48
lIPL	-42	-70	38	39	1.51	4
rIPL	46	-70	38	39	1.91	16

Abbreviations: dMPFC, dorsal medial prefrontal cortex; vMPFC, ventral medial prefrontal cortex; lANG, left angular gyrus; rANG, left angular gyrus; PCC, posterior cingulate cortex/precuneus; lIPL, left inferior parietal lobule; rIPL, right inferior parietal lobule; BA, Brodmann area.

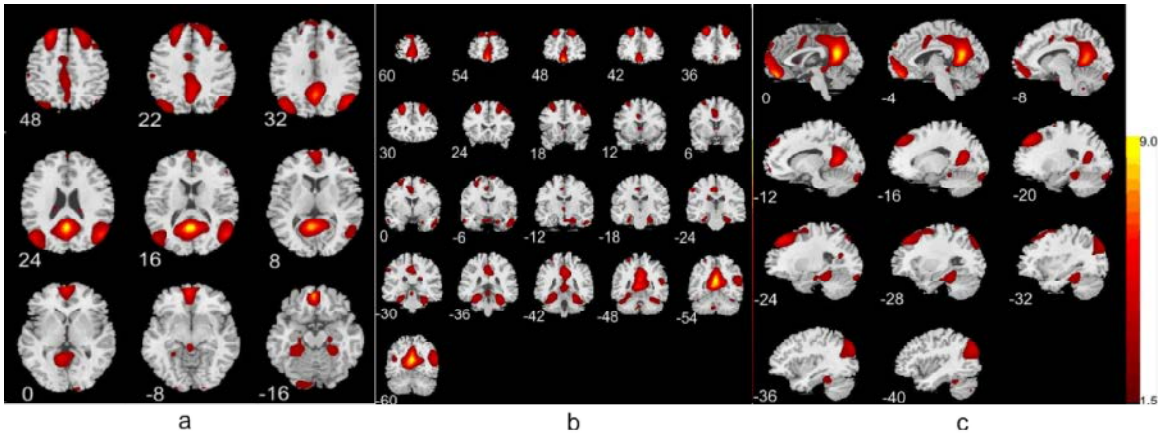

Fig. 1: The spatial independent component (default mode network) of the group results represented with slices.
Images are Z statistics overlaid on the average high-resolution scan transformed into standard (MNI152) space. In the scale bar, the red to yellow colors are Z values, ranging from 1.5 to 9.0. The left hemisphere of the brain corresponds to the left side of the axial slice.

Table 2: Path weights (raw mGCA values) during the resting state. Significant paths ($P< 0.05$) are shown in red.

	PCC	dMPFC	lANG	lIPL	rANG	rIPL	vMPFC
PCC	0.049779	0.016712	0.002784	0.022002	0.018724	0.017581	0.008151
dMPFC	0.017675	0.038342	0.009539	0.013962	0.021969	0.001214	0.020360
lANG	0.001008	0.001483	0.092924	0.072725	0.033542	0.024844	0.010305
lIPL	0.001623	0.001117	0.058540	0.069367	0.021371	0.034247	0.001296
rANG	0.037556	0.001563	0.020932	0.050888	0.084198	0.045259	0.009223
rIPL	0.001430	0.000675	0.014084	0.031940	0.060800	0.085077	0.009580
vMPFC	0.015417	0.028848	0.029576	0.020492	0.021285	0.024958	0.035120

Abbreviations: PCC, posterior cingulate cortex/precuneus; dMPFC, dorsal medial prefrontal cortex; lANG, left angular gyrus; lIPL, left inferior parietal lobule; rANG, left angular gyrus; rIPL, right parietal lobule; vMPFC, ventral medial prefrontal cortex.

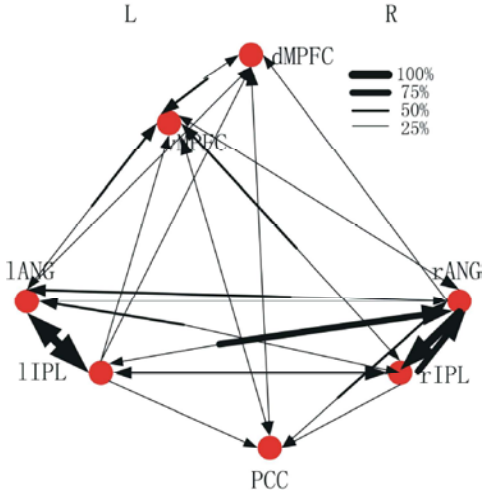

Fig. 2: Causal interactions from the multivariate Granger causality analysis (mGCA).
The relative causal influence strength was divided into four levels (25%, 50%, 75% and 100%) relative to the maximum significant direct directed transfer function (dDTF) value and is represented by the thickness of the black line. Only significant path weights are exhibited in the map (P <.05). Labels and Abbreviations: dMPFC, dorsal medial prefrontal cortex; vMPFC, ventral medial prefrontal cortex; lANG, left angular gyrus; rANG, right angular gyrus; PCC, posterior cingulate cortex/precuneus; lIPL, left inferior parietal lobule; rIPL, right inferior parietal lobule.

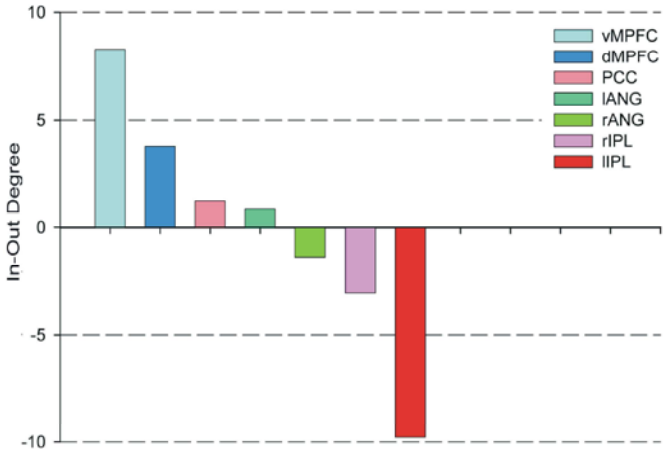

Fig. 3: The In-Out degrees with the path weight of each node in the multivariate Granger causality analysis (mGCA) network are ranked in descending order.
A node with a highly positive In-Out degree is considered to be largely affected by other nodes. On the contrary, a node with negative causal flow exerts a strong causal influence on other ones. Only the brain regions with a nonzero In-Out degree value are listed. Labels and abbreviations are the same as in Fig. 2.

while a connection emerges from the rIPL to the lANG at the strength of 50%. The direct connection from the lIPL to the dMPFC had a weak strength of 25%, while the connections emerging from the rIPL to the dMPFC had strength of 50%. A direct connection emerges from the PCC to the rANG at the strength of 50%, but no direct connection exists between the lANG and PCC. A direct connection emerges from the vMPFC to the rIPL at the weak strength of 25%, but no direct connection exits between the vMPFC and lIPL. In conclusion, the strongest connection is between the lANG and lIPL, but for the PCC, the right hemisphere has stronger connectivity than the left hemisphere. For example, a direct connection emerged from the PCC to the rANG at the strength of 50%, but no direct connections existed between the lANG and PCC (Table 2; Fig. 2).

The activity levels measured by the In-Out degree with path weight varied across the ROIs in the DMN. These brain regions were sorted according to their In-Out degrees of effective connectivity with path weight in descending order: vMPFC > dMPFC > PCC > lANG > rANG > rIPL > lIPL (Fig. 3).

DISCUSSIONS

The remarkable hemispheric asymmetries of the causal influences within the DMN were identified using the mGCA. The results were consistent with previous findings of brain asymmetries and provided further evidence to support the clear asymmetries between the left and right hemispheres [12]. In particular, the current results demonstrating that the left hemisphere, which had stronger dynamic activation than the right hemisphere to the anterior cingulate cortex were consistent with a former study [3].

Investigating resting-state brain networks has recently gained prominence [8]. Many studies have adopted functional connectivity methods [17], which principally focus on connection patterns between a seed region and other brain structures involved in certain functions throughout the brain. However, this method might not directly demonstrate causal interactions between nodes within the network in the brain. Granger causality analyses may be an appropriate method to address this issue. Several metrics of traditional graph-theoretic analyses are used to represent the interactions between the brain regions in the causal connectivity network [21]. The Granger causality method is a basilica approach for detecting the dynamic causal relationships between two time series [22]. However, the model of Granger causality between each node does not take into account the effects of a third brain node, thus it cannot discern the direct or indirect causal connectivity [23]. Therefore, mGCA was introduced to detect the direct causal connections between multiple brain areas and to detect both the direction and strength of the information flow within the brain networks.

The In-Out degrees of the nodes were defined as the difference between each In-degree and Out-degree of the node. If the In-Out degrees were the same for two nodes,

the order was further sorted in descending order in terms of their Out-degree if the In-Out degree was <0, or in ascending order in terms of their In-Out degree if it was >0 [23]. In the current study, the In-Out degrees were weighted with the path and the order was further sorted in descending order. The descending order was highly consistent with a former study [11]. Recently fMRI studies on the DMN demonstrated that a causal target in the neuronal activity propagation process tends to have strong BOLD activity, suggesting that causal influences might predict the neuronal activity levels [16,24,25]. This study also indicated that the power spectral intensity of the mean time series extracted from a brain region was in direct proportion to causal inflows of the brain region. We speculated that the strength of the neural activity would be stronger if the sum of causal inflows with the weight through one node was larger than the other nodes.

CONCLUSIONS

In conclusion, the results of this study have highlighted the presence of clear asymmetries between the left and right brain in the DMN using mGCA. The current findings have significant implications for understanding the functional and structural hemispheric asymmetry when processing information in the human brain. These findings elucidated the dynamical organization of cortical neuronal networks and may provide the foundation for characterizing network disruption in a variety of brain disorders. Furthermore, these findings revealed the causal influences between and among the nodes in the network of the left and right hemispheres.

ACKNOWLEDGEMENTS

This research was supported by “the China Major Project of National Social Science Foundation” (Code: 13&ZD073), “the China Major Project of National Social Science Foundation” (Code: 12&ZD228) and “the China National Key Laboratory of Cognitive Neuroscience and Learning” (CNLZD1304).

REFERENCES

1. Saenger, V.M., F.A. Barrios, M.L. Martínez-Gudiño and S. Alcauter, 2012. Hemispheric asymmetries of functional connectivity and grey matter volume in the default mode network. Neuropsychologia, 50(7): 1308-1315.
2. Toga, A.W. and P.M. Thompson, 2003. Mapping brain asymmetry. Nature Reviews Neuroscience, 4(1): 37-48.
3. Huster, R.J., R. Westerhausen, F. Kreuder, E. Schweiger and W. Wittling, 2007. Morphologic asymmetry of the human anterior cingulate cortex. Neuroimage, 34(3): 888-895.
4. Vernooij, M.W., M. Smits, P.A. Wielopolski, G.C. Houston, G.P. Krestin and A. van der Lugt, 2007. Fiber density asymmetry of the arcuate fasciculus in relation to functional hemispheric language lateralization in both right-and left-handed healthy subjects: a combined fMRI and DTI study. Neuroimage, 35(3): 1064-1076.
5. Gong, G., T. Jiang, C. Zhu, Y. Zang, F. Wang, S. Xie and X. Guo, 2005. Asymmetry analysis of cingulum based on scale-invariant parameterization by diffusion tensor imaging. Human Brain Mapping, 24(2): 92-98.
6. Rose, S., T. Rowland, K. Pannek, A. Coulthard, P. McCombe and R. Henderson, 2012. Structural hemispheric asymmetries in the human precentral gyrus hand representation. Neuroscience, 210: 211-221.
7. Margulies, D.S., A.M. Kelly, L.Q. Uddin, B.B. Biswal, F.X. Castellanos and M.P. Milham, 2007. Mapping the functional connectivity of anterior cingulate cortex. Neuroimage, 37(2): 579-588.
8. Damoiseaux, J.S., S.A.R.B. Rombouts, F. Barkhof, P. Scheltens, C.J. Stam, S.M. Smith and C.F. Beckmann, 2006. Consistent resting-state networks across healthy subjects. Proceedings of the National Academy of Sciences, 103(37): 13848-13853.
9. Fox, M.D., A.Z. Snyder, J.L. Vincent, M. Corbetta, D.C. Van Essen and M.E. Raichle, 2005. The human brain is intrinsically organized into dynamic, anticorrelated functional networks. Proceedings of the National Academy of Sciences of the United States of America, 102(27): 9673-9678.
10. Greicius, M.D., G. Srivastava, A.L. Reiss and V. Menon, 2004. Default-mode network activity distinguishes Alzheimer's disease from healthy aging: evidence from functional MRI. Proceedings of the National Academy of Sciences of the United States of America, 101(13): 4637-4642.
11. Jiao, Q., G. Lu, Z. Zhang, Y. Zhong, Z. Wang, Y. Guo, and Y. Liu, 2011. Granger causal influence predicts BOLD activity levels in the default mode network. Human Brain Mapping, 32(1): 154-161.

12. Yan, H., X.N. Zuo, D. Wang, J. Wang, C. Zhu, M.P. Milham and Y. Zang, 2009. Hemispheric asymmetry in cognitive division of anterior cingulate cortex: a resting-state functional connectivity study. Neuroimage, 47(4): 1579-1589.
13. Liao, W., J. Ding, D. Marinazzo, Q. Xu, Z. Wang, C. Yuan and H. Chen, 2011. Small-world directed networks in the human brain: multivariate Granger causality analysis of resting-state fMRI. Neuroimage, 54(4): 2683-2694.
14. Castelli, F., D.E. Glaser and B. Butterworth, 2006. Discrete and analogue quantity processing in the parietal lobe: A functional MRI study. Proceedings of the National Academy of Sciences of the United States of America, 103(12): 4693-4698.
15. Li, Y.O., T. Adali and V.D. Calhoun, 2006. Sample dependence correction for order selection in fMRI analysis. In Biomedical Imaging: Nano to Macro, 2006. 3rd IEEE International Symposium on (pp: 1072-1075). IEEE.
16. Mantini, D., M.G. Perrucci, C. Del Gratta, G.L. Romani, and M. Corbetta, 2007. Electrophysiological signatures of resting state networks in the human brain. Proceedings of the National Academy of Sciences, 104(32): 13170-13175.
17. Deshpande, G., S. LaConte, G.A. James, S. Peltier and X. Hu, 2009. Multivariate Granger causality analysis of fMRI data. Human brain mapping, 30(4): 1361-1373.
18. Kus, R., M. Kaminski and K.J. Blinowska, 2004. Determination of EEG activity propagation: pair-wise versus multichannel estimate. Biomedical Engineering, IEEE Transactions on, 51(9): 1501-1510.
19. Theiler, J., S. Eubank, A. Longtin and J. Doyne Farmer, 1992. Testing for nonlinearity in time series: the method of surrogate data. Physica D: Nonlinear Phenomena, 58(1): 77-94.
20. Fisher, R.A., 1934. Statistical methods for research workers.
21. Seth, A.K., 2005. Causal connectivity of evolved neural networks during behavior. Network: Computation in Neural Systems, 16(1): 35-54.
22. Roebroeck, A., E. Formisano and R. Goebel, 2005. Mapping directed influence over the brain using Granger causality and fMRI. Neuroimage, 25(1): 230-242.
23. Gao, Q., X. Duan and H. Chen, 2011. Evaluation of effective connectivity of motor areas during motor imagery and execution using conditional Granger causality. Neuroimage, 54(2): 1280-1288.
24. Qi, Z., X. Wu, Z. Wang, N. Zhang, H. Dong, L. Yao and K. Li, 2010. Impairment and compensation coexist in amnestic MCI default mode network. Neuroimage, 50(1): 48-55.
25. Liao, W., D. Mantini, Z. Zhang, Z. Pan, J. Ding, Q. Gong and H. Chen, 2010. Evaluating the effective connectivity of resting state networks using conditional Granger causality. Biological Cybernetics, 102(1): 57-69.